R. L. Ash

AN ANALYSIS OF THE RADIATION FIELD BENEATH A BANK OF TUBULAR QUARTZ-LAMPS

A TECHNICAL REPORT

by

Robert L. Ash

Prepared for the

NATIONAL AERONAUTICS AND SPACE ADMINISTRATION

LANGLEY RESEARCH CENTER

HAMPTON, VIRGINIA 23365

Under

MASTER CONTRACT AGREEMENT NAS1-94

TASK ORDER No. 34

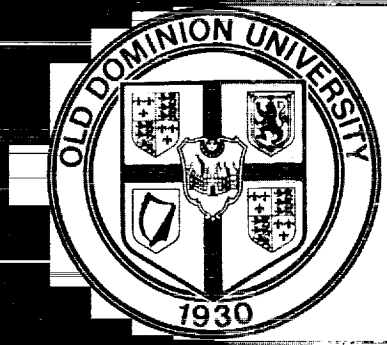

SCHOOL OF ENGINEERING

OLD DOMINION UNIVERSITY

NORFOLK, VIRGINIA

June 1972

Technical Report 72-T3

NAS1-9434-34

AN ANALYSIS OF THE RADIATION FIELD BENEATH A BANK OF TUBULAR QUARTZ LAMPS

A TECHNICAL REPORT

By
Robert L. Ash
Associate Professor of Engineering
School of Engineering
Old Dominion University

Prepared for the
NATIONAL AERONAUTICS AND SPACE ADMINISTRATION
Langley Research Center
Hampton, Virginia 23365

Under
Master Contract Agreement NAS1-9434
Task Order No. 34

Submitted by the
Old Dominion University Research Foundation
P. O. Box 6173
Norfolk, Virginia 23508

June 1972

CONTENTS

FIGURES

AN ANALYSIS OF THE RADIATION FIELD BENEATH A BANK OF TUBULAR QUARTZ LAMPS

By Robert L. Ash[1]

SUMMARY

Equations governing the incident heat flux distribution beneath a lamp-reflector system have been developed. Analysis of a particular radiant heating facility showed good agreement between theory and experiment when a lamp power loss correction was used. In addition, the theory was employed to estimate thermal disruption in the radiation field caused by a protruding probe.

INTRODUCTION

One method for producing relatively high surface heating rates has been to employ banks of tubular, tungsten filament quartz lamps. These lamps are commercially available in lengths[2] of between 12.7 cm and 96.5 cm and are capable of dissipating up to 35 w/cm (ref. 1). By employing a group of these lamps beneath a reflecting panel, surface heating rates in excess of 50 w/cm^2 can be developed.

The purpose of this report is to present a theory which can be used to estimate the incident energy distribution produced by lamp-reflector systems. The configuration under study is shown schematically in figure 1 (p. 2).

For simplicity, it was assumed that the test panel is perfectly absorbing (black) and is at a sufficiently low absolute temperature to neglect radiation back to the reflector. Furthermore, it was assumed that the lamp diameters are small relative to other dimensions of the system and that they do not interfere with the radiant energy passing between reflector and test panel.

---

[1] Associate Professor of Engineering, School of Engineering, Old Dominion University, Norfolk, Virginia 23508.

[2] Length measurements appear in the metric system, 1 centimeter = 0.3937 inch.

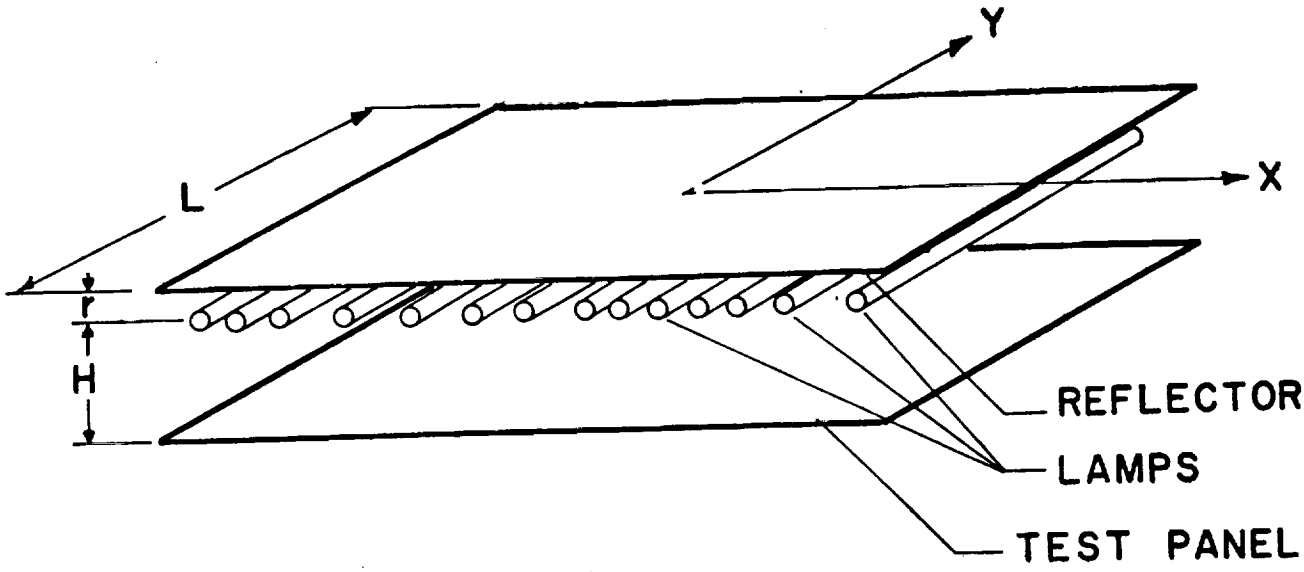

Figure 1.- Schematic view of radiant heating system.

ANALYSIS

It is convenient to focus attention on a single lamp having an arbitrary location beneath a flat reflector panel. Analysis of the radiant energy leaving the lamp can be divided into two parts, direct radiation of the test panel and reflected radiation to the test panel. Direct radiation calculations will be developed first since they can be used to simplify the reflector analysis.

Because the lamp radiates uniformly about its axis, it should be realized that the unit normal on a differential cylindrical surface element is free to rotate in the plane shown in figure 2 (p. 3). A complicated integration can be avoided by using the indirect approach of assuming that the intensity leaving the cylindrical surface element of figure 2 is some known function $I_1(\bar{y})$. That is, $I_1(\bar{y})$ given by

$$I_1(\bar{y}) = I_L(T)\int_0^{2\pi} f(\theta)d\theta \qquad (1)$$

is treated as a known quantity, where $I_L(T)$ is the intensity leaving a differential surface element (rectangular) of the lamp at temperature T and $f(\theta)$ is the function which relates the intensity leaving the differential element to the particular direction under consideration ($f(\theta)$ will be zero for

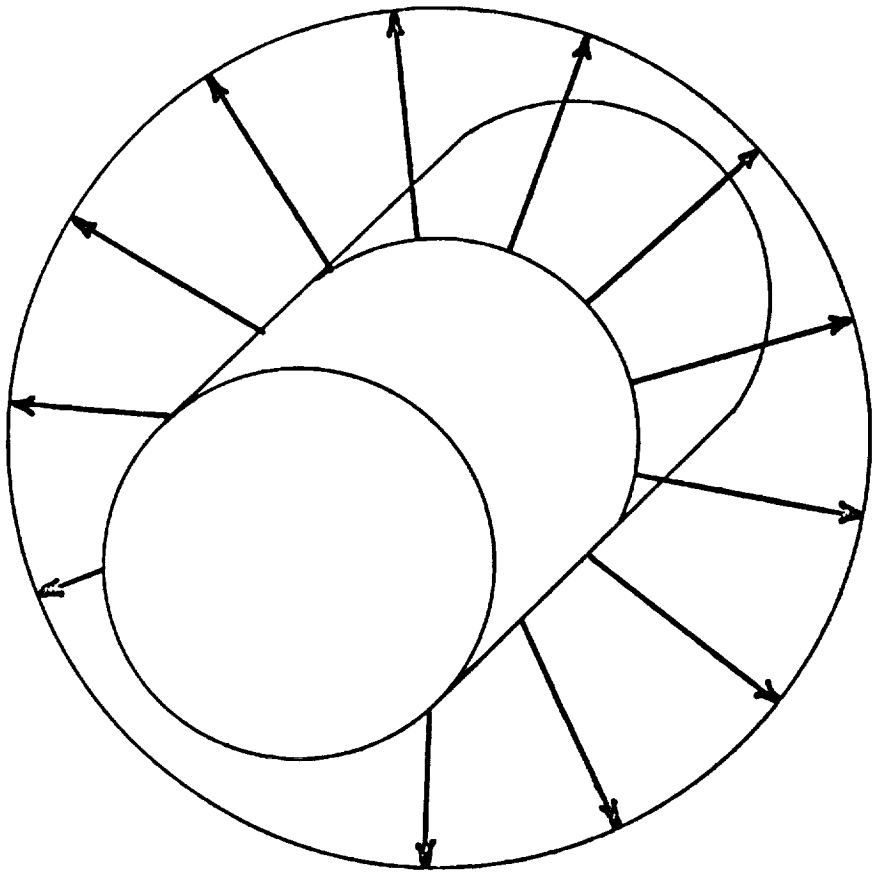

Figure 2.- Plane of radiation symmetry.

some angles since part of the surface is hidden by the lamp filament). It will be convenient to evaluate $I_1(\bar{y})$ later; but it should be noted that, if the lamp is at a uniform temperature, $I_1(\bar{y})$ would be a constant--say I_0.

There are several advantages to this indirect approach. First of all, as has already been mentioned, a difficult integration will at least be postponed. More importantly, by taking advantage of the symmetry of the radiant energy leaving the lamp, it will be possible to ignore the radiation field within the quartz cylinder generated by the tungsten filament. No transmittance calculations are needed. In fact, when the uniform filament temperature assumption is made, it will be found that the filament temperature itself is not needed in the calculations. More precisely, it will be possible to relate directly I_0 to the total power dissipated by the lamp.

Direct Radiation from a Lamp at Uniform Temperature

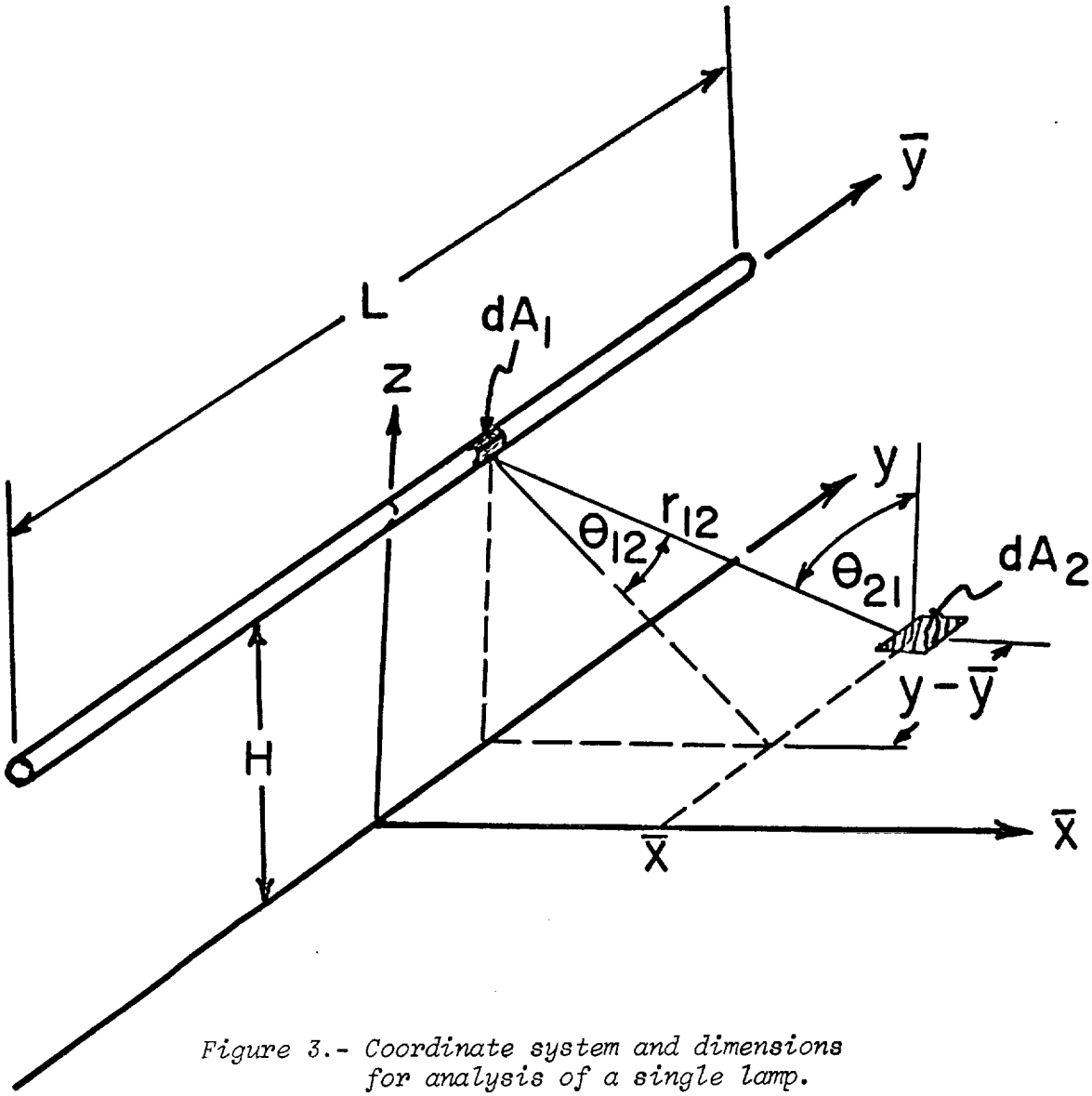

Figure 3.- Coordinate system and dimensions for analysis of a single lamp.

From figure 3, the incident flux on the test panel $f_2(\bar{x},y)$ is given by

$$f_2(\bar{x},y) = \int_{-\frac{L}{2}}^{\frac{L}{2}} \frac{I_1(\bar{y}) \cos \theta_{12} \cos \theta_{21}}{r_{12}^2} D d\bar{y} \tag{2}$$

$$= DHI_0(\bar{x}^2 + H^2)^{\frac{1}{2}} \int_{-\frac{L}{2}}^{\frac{L}{2}} \frac{d\bar{y}}{[\bar{x}^2 + H^2 + (y - \bar{y})^2]^2}$$

where D is the lamp diameter. This equation can be rewritten in terms of the dimensionless variables $\bar{f}_2$, $\bar{\xi}$, ζ, $\bar{\zeta}$, and γ, defined by

$$\bar{f}_2(\bar{\xi},\zeta) = \frac{f_2(\bar{x},y)}{\pi I_o}\frac{H}{D}$$

$$\bar{\xi} = \frac{\bar{x}}{H}$$

$$\zeta = \frac{y}{L} \tag{3}$$

$$\bar{\zeta} = \frac{\bar{y}}{L}$$

and

$$\gamma = \frac{L}{H}$$

Furthermore, equation (2) can be integrated leaving

$$\bar{f}_2(\bar{\xi},\zeta) = \frac{1}{2\pi(\bar{\xi}^2+1)}\left[\frac{\gamma(\zeta+\tfrac{1}{2})(\bar{\xi}^2+1)^{\frac{1}{2}}}{\bar{\xi}^2+1+\gamma^2(\zeta+\tfrac{1}{2})^2} - \frac{\gamma(\zeta-\tfrac{1}{2})(\bar{\xi}^2+1)^{\frac{1}{2}}}{\bar{\xi}^2+1+\gamma^2(\zeta-\tfrac{1}{2})^2} + \tan^{-1}\frac{\gamma(\zeta+\tfrac{1}{2})}{(\bar{\xi}^2+1)^{\frac{1}{2}}} - \tan^{-1}\frac{\gamma(\zeta-\tfrac{1}{2})}{(\bar{\xi}^2+1)^{\frac{1}{2}}}\right] \tag{4}$$

The virtual intensity I_o can be related to the lamp power by realizing that one-eighth of the total energy radiated by the lamp $(q_o/8)$ is incident on the test surface region given by $0 \leq y < \infty$, $0 \leq \bar{x} < \infty$.

Hence,

$$\int_0^\infty\int_0^\infty f_2(\bar{x},y)\,d\bar{x}\,dy = \gamma\pi HDI_o\int_0^\infty\int_0^\infty \bar{f}_2(\bar{\xi},\zeta)\,d\bar{\xi}\,d\zeta = \frac{q_o}{8} \tag{5}$$

or

$$\int_0^\infty\int_0^\infty \bar{f}_2(\bar{\xi},\zeta)\,d\bar{\xi}\,d\zeta = \frac{q_o}{8\pi I_o HD\gamma} \tag{6}$$

Equation (6) can be integrated directly to yield

$$\frac{\pi}{8} = \frac{q_o}{8\pi DHI_o\gamma} \tag{7}$$

leaving

$$I_o = \frac{q_o}{\pi DL}\frac{1}{\pi} \tag{8}$$

Now, when the lamp is at a uniform temperature and there is no radiation from the surroundings,

$$\frac{q_o}{\pi DL} = \varepsilon\sigma T_o^4 \tag{9}$$

Furthermore,

$$\pi I_o = \varepsilon\sigma T_o^4 \tag{10}$$

Though these last two relations are interesting, their usefulness is limited since they relate temperature to heating rate and yield an apparent emissivity for the cylindrical element when the temperature is known. There is no well defined temperature or emissivity because both quartz cylinder and tungsten filament emit radiant energy at different temperatures with different emissivities, to say nothing of the transmittance through quartz.

If the *nth* lamp is located at a distance x_n from the reference edge of the reflector, $\bar{x}$ is related to the reflector coordinate x by

$$\bar{x} = x - x_n \tag{11}$$

Similarly,

$$\bar{\xi} = \xi - \xi_n \tag{12}$$

where

$$\xi = \frac{x}{H}$$

and

$$\xi_n = \frac{x_n}{H}$$

If a new variable η_n is defined by

$$\eta_n = (\bar{\xi}^2 + 1)^{\frac{1}{2}} \tag{13}$$

the incident flux produced by the *nth* lamp is given by

$$f_n(x,y) = \frac{q_o}{H^2} F(x,y;x_n,H) \tag{14}$$

where

$$F(x,y;x_n,H) \equiv \frac{1}{2\pi^2\eta_n}\left\{\frac{\gamma(\zeta+\frac{1}{2})}{\eta_n^2+\gamma^2(\zeta+\frac{1}{2})^2} - \frac{\gamma(\zeta-\frac{1}{2})}{\eta_n^2+\gamma^2(\zeta-\frac{1}{2})^2} + \frac{1}{\eta_n}\left[\tan^{-1}\frac{\gamma(\zeta+\frac{1}{2})}{\eta_n} - \tan^{-1}\frac{\gamma(\zeta-\frac{1}{2})}{\eta_n}\right]\right\} \tag{15}$$

and η_n, γ, and ζ are defined by

$$\eta_n \equiv \left[(x - x_n)^2 + H^2\right]^{\frac{1}{2}}/H \tag{16a}$$

$$\gamma = L/H \tag{16b}$$

and

$$\zeta = y/L \tag{16c}$$

$F(x,y;x_n,H)$ shall be called the *radiation function.*

Reflected Radiation Contribution

Reflected contribution to the energy distribution on the test panel can be developed conveniently from the previous calculations. If the reflector is assumed to act as a combination specular and diffuse surface, the reflectivity ρ can be written

$$\rho = \rho^d + \rho^s \tag{17}$$

where ρ^s is the specular reflection component and ρ^d is the diffuse component. Separate analyses are required for the specular and diffuse contributions.

The specular contribution can be developed directly from the previous direct radiation analysis. That is, if the distance from the lamps to the reflector panel is R, a set of imaginary lamps located at a distance H + 2R above the test panel and having strength I_s given by

$$I_s = \rho^s I_o \tag{18}$$

represent the radiant energy caused by specular reflection from the test panel.

If the specular contribution of the *nth* lamp to the incident flux at the test panel is designated $f_n^s(x,y)$, it should be obvious that

$$f_n^s(x,y) = \frac{\rho^s q_o}{(H + 2R)^2} F(x,y;x_n,H + 2R) \tag{19}$$

In order to calculate the diffusely reflected energy contribution, it is first necessary to calculate the incident energy distribution on the reflector panel. Again, the incident energy function can be developed directly from the *radiation function*. In this case, the *test surface* is located at a distance R from the lamps and the incident flux on the reflector panel is given by

$$B_n(x,y) = \frac{q_o}{R^2} F(x,y;x_n,R) \tag{20}$$

Consequently, the intensity leaving a point on the reflector panel would be $\rho^d B_n(x,y)/\pi$ and the incident flux on the test panel due to diffuse reflection from the *nth* lamp would be

$$f_n^d(x,y) = \frac{\rho^d}{\pi} \underset{\substack{\text{reflector} \\ \text{area}}}{\iint} \frac{B_n(u,v) \cos \theta_{RT} \cos \theta_{TR}}{r_{RT}^2} dudv \tag{21}$$

where Θ_{RT} and Θ_{TR} are the angles between normals at the reflector and test panel and the radius r_{TR}. From this particular geometry,

$$\cos \Theta_{RT} = \cos \Theta_{TR} = (R + H)/r_{TR} \tag{22}$$

where

$$r_{TR}^2 = (R + H)^2 + (x - u)^2 + (y - v)^2 \tag{23}$$

From equations (22) and (23), the incident energy on the test surface can be written

$$f_n^d(x,y) = \frac{q_o}{R^2}\frac{\rho^d}{\pi}(R + H)^2 \iint \frac{F(u,v;x_n,R)dudv}{[(R + H)^2 + (x - u)^2 + (y - v)^2]^2} \tag{24}$$

Because of the form of $F(u,v;x_n,R)$ in equation (15), equation (24) is a hyperelliptic integral and must be integrated numerically. A computer program has been written to evaluate equation (24), using an equally spaced grid network. The integral has been approximated by

$$\frac{(R + H)^2}{\pi} \iint \frac{F(u,v;x_n,R)dudv}{[(R + H) + (x - u)^2 + (y - v)^2]^2}$$

$$\underset{\sim}{=} F_\Sigma(x,y;x_n,R,H)$$

$$= \frac{(R + H)^2}{\pi} \sum_{i=1}^{N_I} \sum_{j=1}^{N_J} \frac{F(u_i,v_j,x_n,R)\Delta u \Delta v}{[(R + H)^2 + (x - u_i)^2 + (y - v_j)^2]^2} \tag{25}$$

where F_Σ has been defined for convenience and N_I and N_J represent the number of reflector surface elements in the x and y directions, respectively.

At this point, the incident heat flux due to the *nth* lamp located at some distance x_n from the reflector reference line can be written

$$f_n^T(x,y) = q_o\left[\frac{F(x,y;x_n,H)}{H^2} + \frac{\rho^s F(x,y;x_n,H + 2R)}{(H + 2R)^2} + \frac{\rho^d F_\Sigma(x,y;x_n,R,H)}{R^2}\right]$$

$$= \frac{q_o}{H^2}\left[F(x,y;x_n,H) + \gamma_s \rho^s F(x,y;x_n,H + 2R) + \gamma_d \rho^d F_\Sigma(x,y;x_n,R,H)\right]$$

where

$$\gamma_s = \left(\frac{H}{H + 2R}\right)^2$$

and

$$\gamma_d = \left(\frac{H}{R}\right)^2.$$

Finally, the incident heat flux caused by combined radiation from an array of N lamps is given by

$$q(x,y) = \sum_{n=1}^{N} f_n^T(x,y)$$

$$= \frac{q_o}{H^2} \sum_{n=1}^{N} \left[F(x,y;x_n,H) + \gamma_s \rho^s F(x,y;x_n,H + 2R) + \gamma_d \rho^d F_\Sigma(x,y;x_n,R,H) \right] \tag{27}$$

An experimental investigation has been carried out to determine the accuracy of this model and will be discussed further in the experimental section. A computer program for evaluating equation (27) when $\rho^s = 0$ is given in appendix A.

EXPERIMENT

The lamp-reflector system studied was located at the National Aeronautics and Space Administration, Langley Research Center and was used for the study of space shuttle material candidates. The system was designed to produce a nearly uniform radiant heat flux over a 5-cm by 5-cm area in an effort to simulate multiple reentry conditions.

Essentially, the system consisted of 45 cylindrical, tungsten filament lamps mounted beneath a water-cooled aluminum reflector similar to the schematic shown in figure 1 (p. 2). The lamp-reflector system was mounted on a water-cooled aluminum table and could be adjusted vertically on the table. The lamps were mounted in water-cooled copper brackets and equally spaced 1.27 cm apart. The distance between the plane of the lamp centerlines and the reflector was 3.3 cm.

Power was supplied to the lamps by a balanced three-phase system which supplied each group of 15 lamps (1-15, 16-30, and 31-45) with nominally the same power. The power consumption was measured by monitoring the phase voltage and current.

The incident heat flux was measured with calibrated thin-foil, Gardon-type, heat flux sensors with foil diameters of 0.635 cm and surface emissivities of 0.89. The sensors were mounted in a low thermal-conductivity block, which positioned the sensing foil 5.08 cm above the water-cooled table. The heat flux

sensors were positioned on the horizontal plane by means of a grid system which had been inscribed on the surface of the table.

The major difficulty in comparing theory with experimental data rested in separating the energy which was radiated by the lamps from the energy conducted through the lamp mounts and from the energy carried away convectively by the air. Only the radiant energy leaving the lamps was included in the theory.

Initially, energy balances were made on the cooling water passing through the copper lamp mounts to determine conduction loss. However, cooling water data were not accurate because the brackets were heated by radiation and were receiving energy by conduction from the lamps. The final procedure consisted of measuring the conduction-convection loss experimentally.

The experimental procedure employed assumed that theory and data agreed at a selected data point. By forcing agreement at the particular data point, a q_0 (power radiated by each lamp) could be calculated and the difference between the calculated q_0 and the power supplied to each lamp $\left(\frac{\text{total power supplied}}{\text{total number of lamps}}\right)$ was defined as the unradiated energy or power loss.

Unfortunately, power loss was affected by the spacing between the lamp-reflector system and the water-cooled table. As the distance between the table and lamps was decreased, the lamp temperatures increased and the conduction and convection losses increased. In addition, radiation loss resulting from multiple reflections between table, which was not perfectly absorbing, and reflector changed with spacing. All of these factors affected the calibration.

Since most of the tests conducted at this facility positioned the specimen surface either 8.9 cm or 5.08 cm from the test surface, conduction corrections were developed for these distances. The data were gathered when the heat flux sensor was located at 8.9 cm from the lamp plane and a detailed check was made at a single power setting at 5.08 cm. The conduction correction data are shown in figure 4 (p. 11).

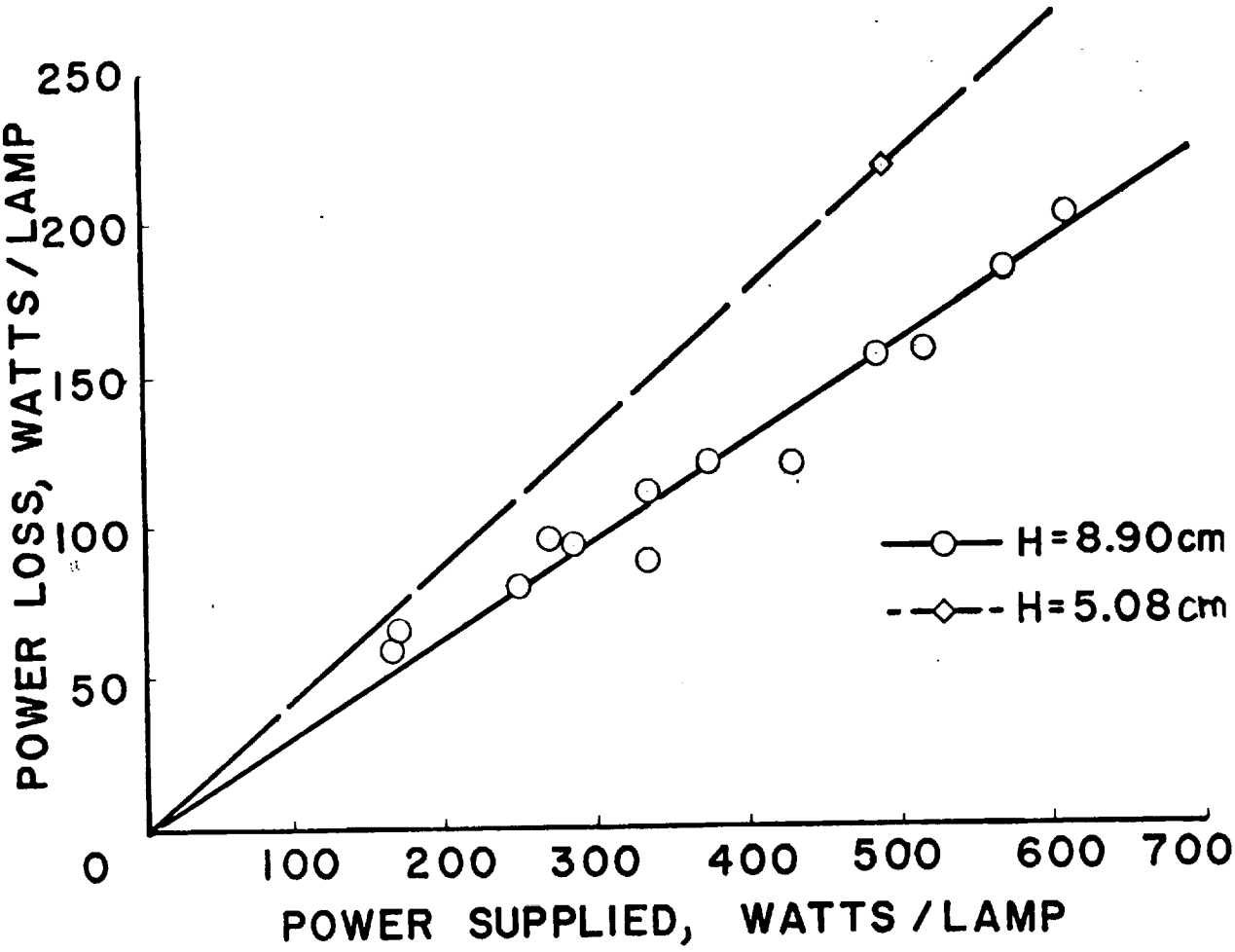

Figure 4.- Power loss correction.

In order to verify the validity of the conduction correction, additional measurements were taken with the heat flux sensor in the reference position, but varying the lamp configuration. Using a power setting which nominally supplied 495 total watts to each lamp when the lamps were 5.08 cm above the sensor surface, two tests were run with 30- and 33-lamp configurations in place of the original 45. The 30-lamp configuration was produced by removing 15 lamps from their brackets so that there were 10 lamps equally spaced 1.27 cm apart, a gap of 7.62 cm, 5 lamps 1.27 cm apart, a gap of 7.62 cm, 5 lamps 1.27 cm apart, a gap of 7.62 cm, and 10 lamps 1.27 cm apart. The 33-lamp configuration was produced by replacing one lamp at the center of each of the 7.62-cm gap. The three test configurations are shown schematically in figure 5 (p. 12) along with the theoretically predicted heat flux distributions.

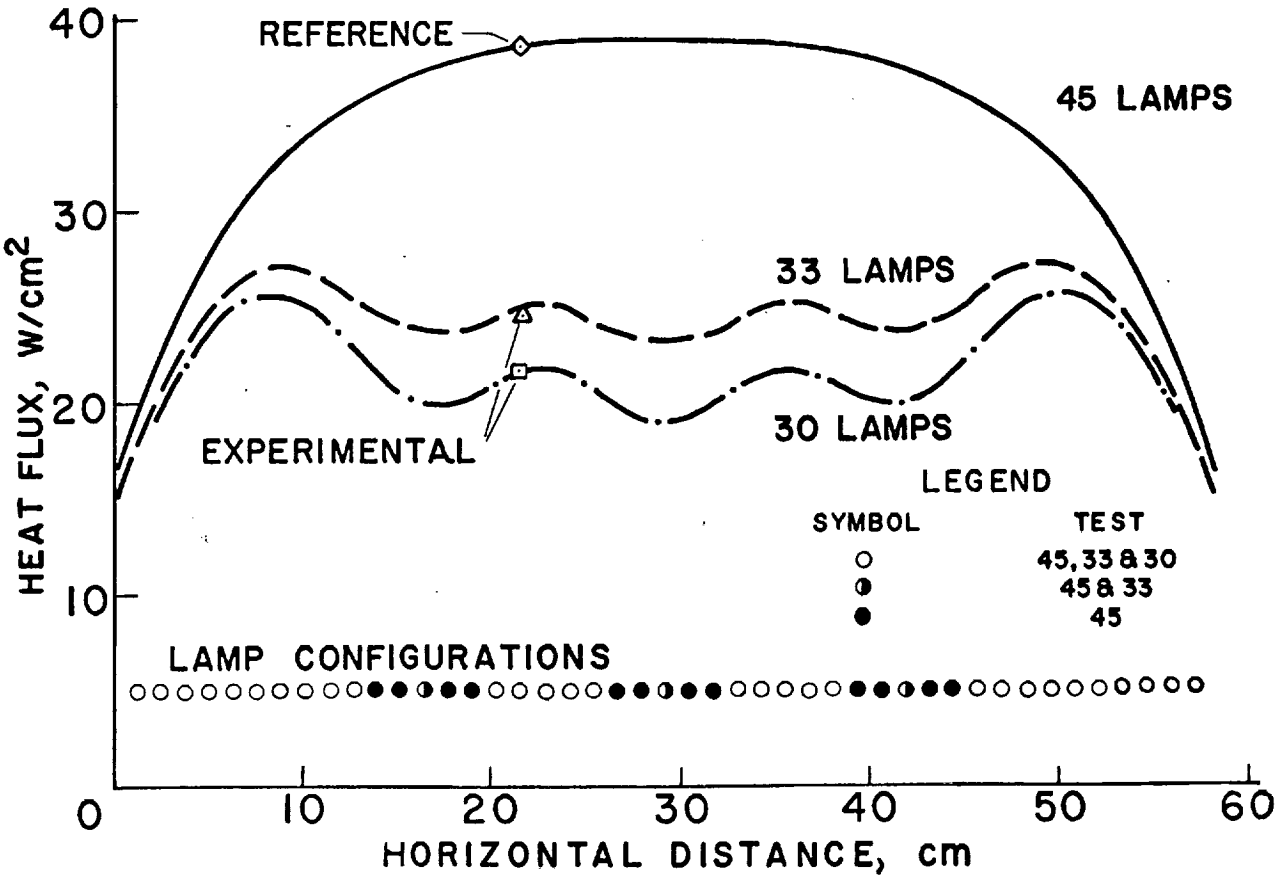

Figure 5.- Heat flux measurements and distributions for calibration experiments.

The data point marked *reference* in figure 5 was used to develop the power loss correction shown in figure 4 (p. 11). The calculated 45-lamp power loss was 218 watts per lamp. Hence, the value of q_0 for each of the lamps was 277 watts. Using that value in the theoretical calculations, distributions shown in figure 5 were generated. The differences between predicted and measured heat fluxes in the 30- and 33-lamp configurations were -1 percent and +2.5 percent, respectively.

Obviously, the above correction procedure makes the theory appear more accurate than it is in reality. However, the data gathered in a previous test, which employed the 45-lamp configuration 5.08 cm above the test surface, verify the fact that measured and predicted incident flux distributions are in close agreement when the power loss correction is used. The flux was measured in the x and y directions, 2.54 cm off the centerline in both cases. The power loss was taken directly from figure 4 and no attempt was made to match data. The measured and theoretical distributions are shown in figures 6 and 7 (p. 13). It can be seen that theory predicts both heat flux magnitude and distribution.

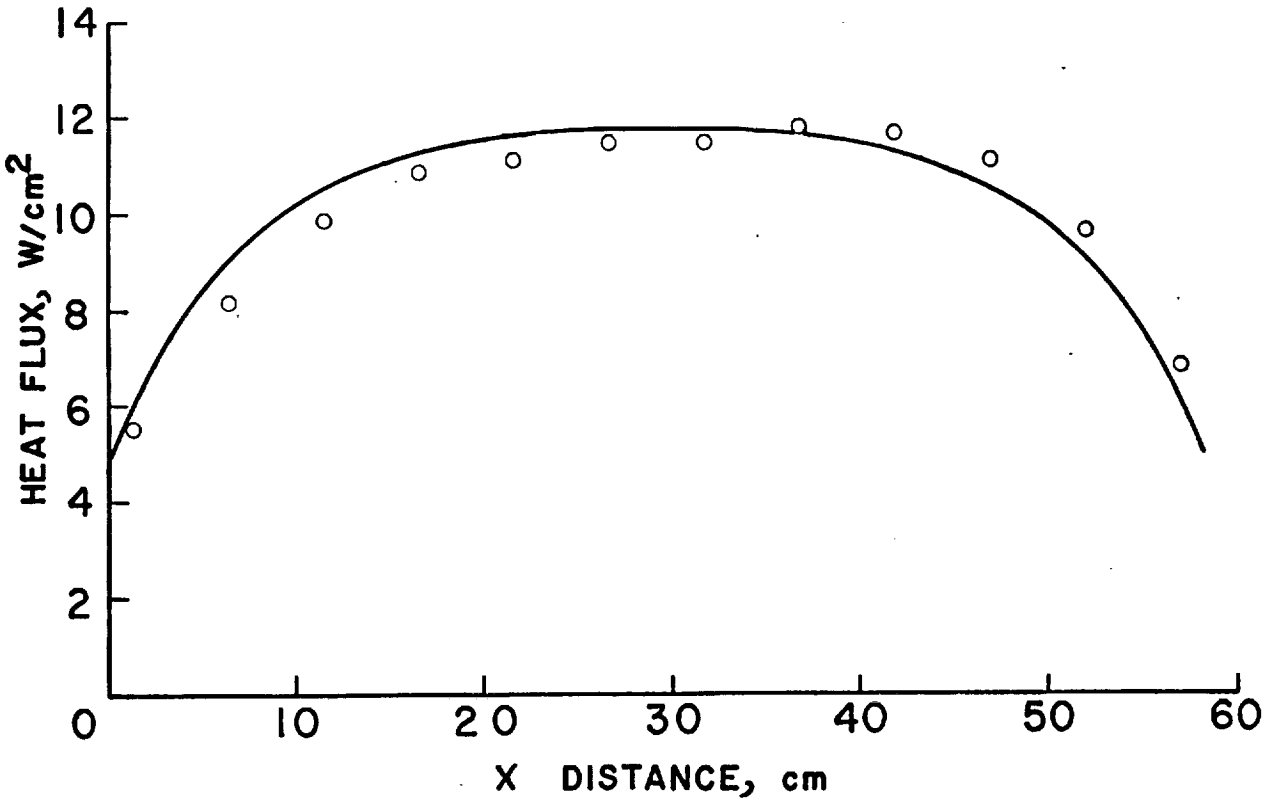

Figure 6.- Measured and theoretical heat flux distributions for a 45-lamp test. (H = 5.08 cm. y to $y_{centerline}$ = 2.54 cm)

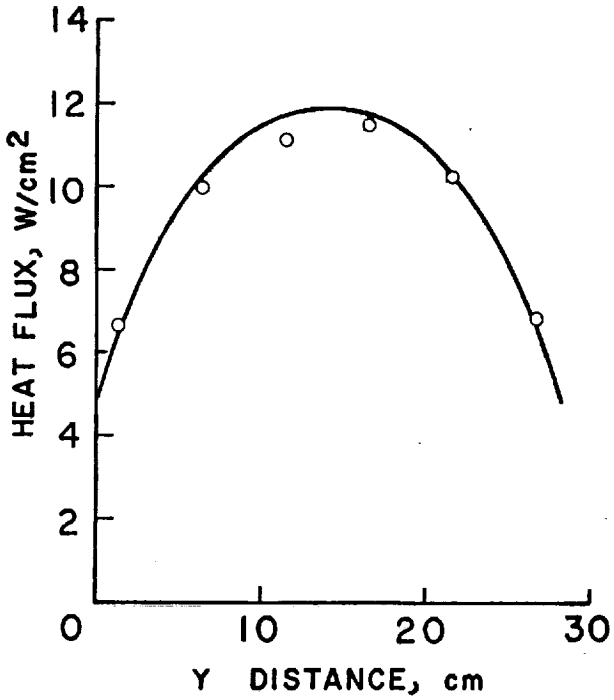

Figure 7.- Measured and theoretical heat flux distributions for a 45-lamp test. (H = 5.08 cm. x to $x_{centerline}$ = 2.54 cm)

From the experimental results discussed in this section, it can be concluded that theory and experiment show good agreement. The correction factor employed in the analysis probably overcorrects the theory and, therefore, restricts quantitative accuracy statements. However, data gathered for the three configurations indicated that the correction is valid, at least for these particular lamp configurations.

THERMAL DISRUPTION DUE TO A PROTRUDING PROBE

One proposed method for measuring surface temperatures in the previously described radiation facility utilizes a protruding cylindrical probe. The probe configuration is shown schematically in figure 8.

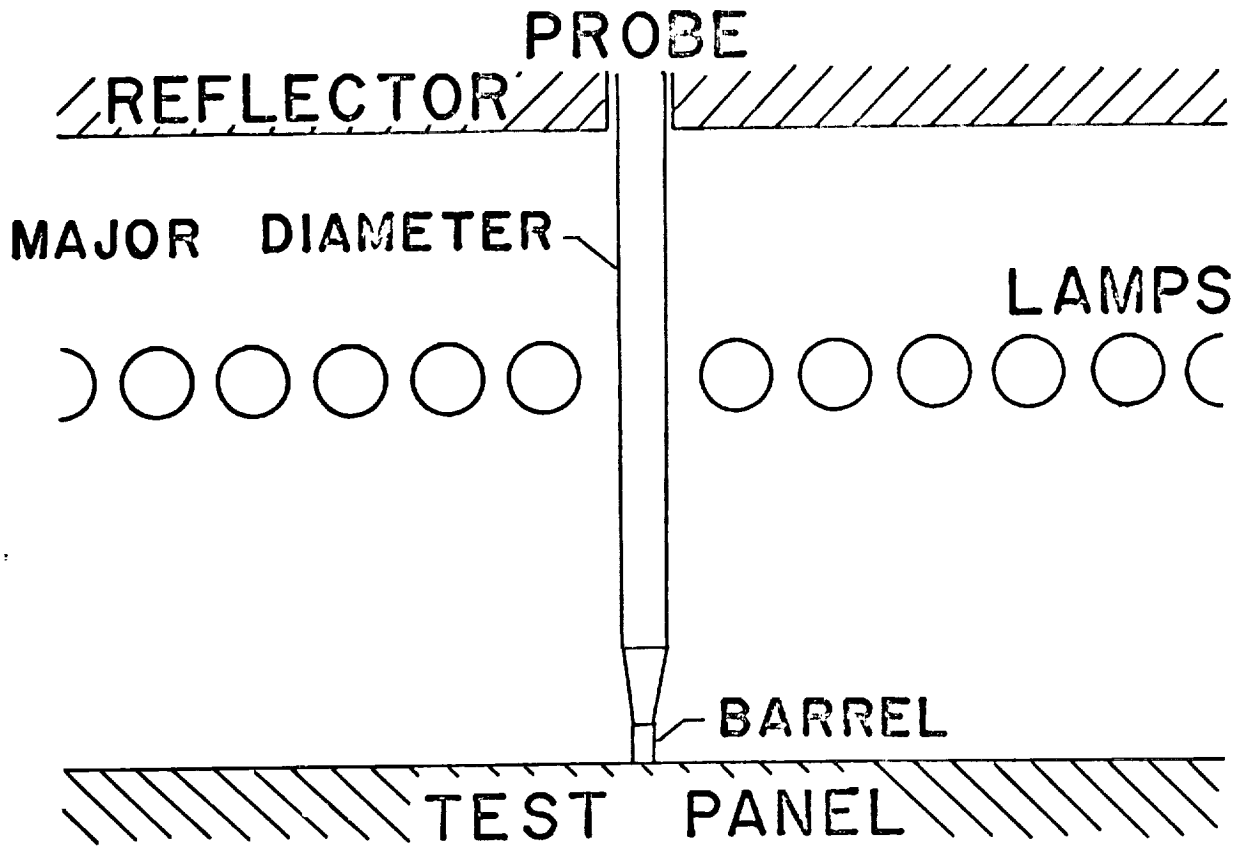

Figure 8.- Full-scale view of probe protruding through center of reflector.

Essentially, a hole will be cut in the center of the reflector to allow the probe to extend through the radiation field. The probe will be lowered through the hole until it contacts the test surface and remain there long

enough to record the surface temperature. Then, the probe will be removed to permit uniform radiant heating. The question is, how will the radiation field be affected in the vicinity of the probe during the time the probe is lowered in the field?

When the probe is in contact with the test surface, no radiation is received directly beneath the probe. In addition, the surface in the vicinity of the probe is obscured from some parts of the lamp-reflector system. If the probe is assumed black and nonradiating, determination of thermal disruption is straightforward, though tedius.

The previous program for calculating incident heat flux distribution has been modified to determine disruption caused by the probe. Essentially, the image of the probe, as seen from the center of a particular test surface element (an arbitrary surface element from the original computations), was projected back into the lamp and reflector planes. Location and dimensions of the obscured lamp segments as well as locations of the obscured reflector surface elements were then computed.[1] Then, the radiant energy arriving at the test surface element from the obscured lamp and reflector elements was computed and subtracted from the original undisturbed heat flux value. The complete program for making these calculations is included in appendix A.

The central region of the particular configuration studied is shown approximately to scale in figure 8 (p. 14). The lamps were 5.080 cm from the test surface. The probe had a major diameter of 0.660 cm, a barrel length of 0.508 cm, and a barrel diameter of 0.254 cm. The length of the taper from the major diameter to the barrel was 1.016 cm. In the computer calculations, the center lamp was removed from each of the three phases, leaving 42 lamps. The center lamp was removed from the center phase to permit the probe to be located in the center of the radiation field, while the center lamps were removed from the other two phases to balance the power consumption. The ratio of the disrupted heat flux to the undisturbed heat flux in the vicinity of the probe is shown in figures 9 and 10 (p. 16).

Figures 9 and 10 indicate that significant variations in the incident heat flux are confined to a very small region in the vicinity of the probe. The radiation field is depressed only slightly at distances greater than about 1 cm from the probe. Furthermore, the actual heat flux depression should be

[1] A reflector element was considered obscured if its center were obscured.

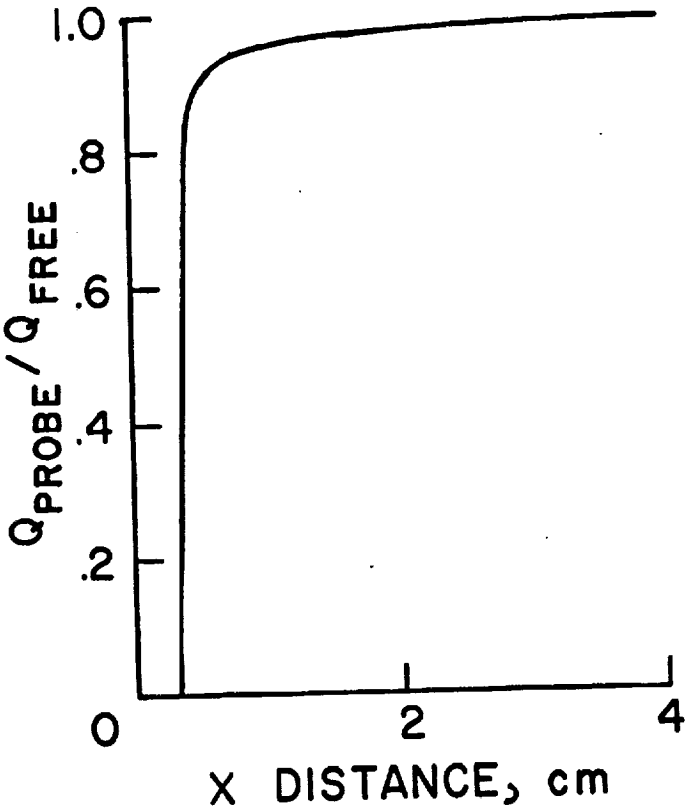

Figure 9.- Ratio of disturbed incident heat flux to undisturbed heat flux along the x axis in the vicinity of a probe whose major diameter is 0.66 cm. The probe is located at the center of the lamp-reflector system.

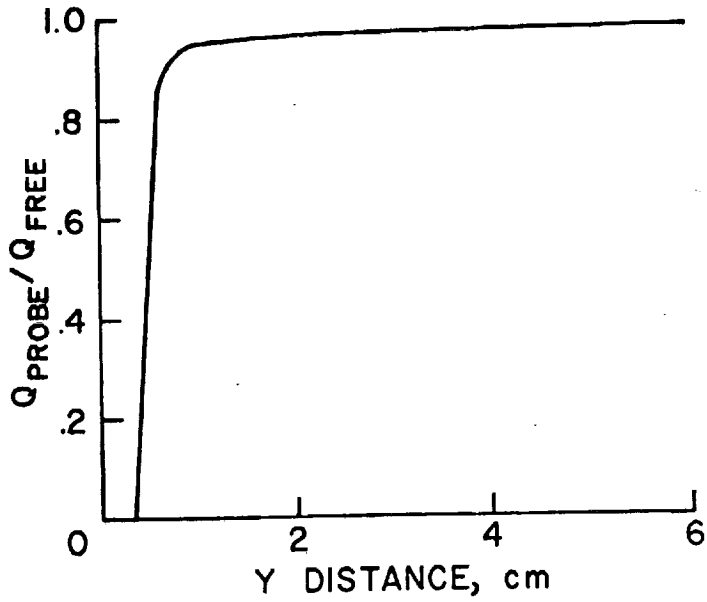

Figure 10.- Ratio of disturbed incident heat flux to undisturbed heat flux along the y axis in the vicinity of a probe whose major diameter is 0.66 cm. The probe is located at the center of the lamp-reflector system.

less than that shown because some radiant energy will be reflected from the probe to the test surface and that reflected radiant energy has not been included in the present analysis.

CONCLUSIONS

From comparison of experimental and theoretical results, it can be concluded that the present theory is a reasonable approximation of the actual radiation field produced by a bank of tubular lamps. The theory accurately predicted the dimensionless variation in heat flux with location for the lamp-reflector systems studied. However, a lamp power correction was required to yield close numerical agreement. It has been shown that this procedure may be useful in designing specified radiation heat flux distributions (appendix B), although additional work is required to develop two-dimensional design capabilities.

Finally, the theory has been used to show that heat flux distribution is only slightly altered in the vicinity of a protruding cylindrical probe. Accuracy of these calculations must be validated by experiment.

APPENDIX A

COMPUTER PROGRAM

The FORTRAN IV computer program for calculating incident heat flux from a lamp-reflector system is incorporated in this appendix. Included is the program for calculating reduced incident heat flux caused by a probe protruding through the center of the lamp-reflector system.

```
//ODASH JOB (0977,0404,65,3),'ROBERT',MSGLEVEL=(2,0),CLASS=T
// EXEC FORTGCLG
//FORT.SYSIN DD *
      REAL L
      DIMENSION DIR(92,44),DDIF(92,44),XI(45),HI(4)
C     N=NUMBER OF LAMPS
      N=42
C     R=HEIGHT OF REFLECTOR ABOVE LAMPS
      R=1.3
C     L=LENGTH OF LAMP HEATING ELEMENT
      L=10.
C     RHO=REFLECTOR REFLECTIVITY
      RHO=0.95
C     READ IN SPATIAL DISTRIBUTION OF LAMPS
      DO 2 I=1,N
      READ(5,1) XI(I)
    1 FORMAT(F15.8)
    2 CONTINUE
C     H=HEIGHT OF LAMPS ABOVE TEST SURFACE
      H=2.
C     INITIALIZATION OF DIR AND DDIF
      DO 4 I=1,92
      DO 3 J=1,44
      DIR(I,J)=0.
      DDIF(I,J)=0.
    3 CONTINUE
    4 CONTINUE
      WRITE(6,500)H,N
  500 FORMAT(5X,'H= ',F6.2,10X,'N= ',I5,//)
C     CALCULATION OF THE DIRECT INCIDENT INTENSITIES ON THE TEST SURFACE
C          AND THE REFLECTOR
C     DX=GRID SPACING IN THE X-DIRECTION
      DX=.25
C     DY=GRID SPACING IN THE Y-DIRECTION
      DY=.25
      DX2=DX/H
      DXR=DX/R
      DY2=DY/L
      GAM=L/H
      GAR=L/R
      GAD=(H/R)**2
      DO 7 K=1,N
```

```
      DO 6 I=1,92
      DO 5 J=1,44
      CI=I
      CJ=J
      CI=CI-.5
      CJ=CJ-.5
      X=CI*DX2
      Y=CJ*DY2-.55
      GA=GAM
      XL=XI(K)/H
      CALL FICT(X,Y,XL,GA,DI)
      DIR(I,J)=DIR(I,J)+DI
C     INCIDENT REFLECTOR INTENSITY IS CALCULATED BY TREATING IT AS A
C          TEST SURFACE
      X=CI*DXR
      GA=GAR
      XL=XI(K)/R
      CALL FICT(X,Y,XL,GA,DI)
      DDIF(I,J)=DDIF(I,J)+DI
    5 CONTINUE
    6 CONTINUE
    7 CONTINUE
C     CALCULATION OF IRRADIATION AT SELECTED POINTS
      DO 11 I=1,46
      DO 10 J=2,22,4
      CI=I
      CJ=J
      CI=CI-.5
      CJ=CJ-.5
      X=CI*DX2
      Y=CJ*DY2-.55
C     X AND Y ARE THE DIMENSIONLESS COORDINATES OF THE POINT ON THE TEST
C          PANEL
      DO 9 II=1,92
      DO 8 JJ=1,44
      CII=II
      CJJ=JJ
      CII=CII-.5
      CJJ=CJJ-.5
      XX=CII*DX2
      YY=CJJ*DY2-.55
C     XX AND YY ARE THE DUMMY VARIABLES USED IN THE REFLECTOR
C          INTEGRATION ROUTINE
      PI=3.1415926
      RHM=(1.+R/H)**2
      XDS=(X-XX)**2
      YDS=(GAM*(Y-YY))**2
      PREF=GAD*GAM*RHM*RHO*DX2*DY2/PI
      DEN=(RHM+XDS+YDS)**2
      REFL=PREF*DDIF(II,JJ)/DEN
      DIR(I,J)=DIR(I,J)+REFL
    8 CONTINUE
```

```
    9 CONTINUE
   10 CONTINUE
      WRITE(6,100)DIR(I,2),DIR(I,6),DIR(I,10),DIR(I,14),DIR(I,18),DIR(I,
     122)
  300 FORMAT(E16.8)
  100 FORMAT(6E16.8)
  200 CONTINUE
   11 CONTINUE
  110 CONTINUE
      DO 1100 I=46,53
      DO 1000 J=16,22
      IF(J-18)949,948,947
  947 IF(J-22)949,948,949
  948 IF(I-46)950,950,949
  949 CONTINUE
      CI=I
      CJ=J
      CI=CI-.5
      CJ=CJ-.5
      X=CI*DX2
      Y=CJ*DY2-.55
      DO 900 II=1,92
      DO 800 JJ=1,44
      CII=II
      CJJ=JJ
      CII=CII-.5
      CJJ=CJJ-.5
      XX=CII*DX2
      YY=CJJ*DY2-.55
      XDS=(X-XX)**2
      YDS=(GAM*(Y-YY))**2
      PREF=GAD*GAM*RHM*RHO*DX2*DY2/PI
      DEN=(RHM+XDS+YDS)**2
      REFL=PREF*DDIF(II,JJ)/DEN
      DIR(I,J)=DIR(I,J)+REFL
  800 CONTINUE
  900 CONTINUE
  950 CONTINUE
 1000 CONTINUE
 1100 CONTINUE
C     PROBE SHADOW PROBLEM
C
C     PROBE DIMENSIONS
C     A=LENGTH OF CONICAL SECTION BETWEEN MAJOR DIAMETER AND BARREL (IN.
      A=0.4
C     B=BARREL LENGTH LENGTH (IN.)
      B=0.2
C     C=BARREL DIAMETER (IN.)
      C=0.1
C     D=MAJOR DIAMETER (IN.)
C     PROGRAM IS OPERABLE ONLY IF D IS LESS THAN 0.50 INCH.
      D=0.26
```

```
C     REDUCED INCIDENT HEAT FLUX WILL BE CALCULATED FOR I=46-52, J=16-22
      RC=C/2.
      RD=D/2.
      HIN=H
      XCL=11.375
      DO 103 I=46,52
      DO 104 J=16,22
      ICONT=0
      IWARN=0
      H=HIN
      CI=I
      CJ=J
      X=(CI-0.5)*0.25
      Y=(CJ-0.5)*0.25-5.5
      WRITE(6,600)X,Y,DIR(I,J)
  600 FORMAT(/,5X,'X= ',F10.4,5X,'Y= ',F10.4,5X,'ORIGINAL Q= ',E16.8)
      IF(I-46)105,106,105
  106 IWARN=1
C     IF PROBE DIAMETER EXCEEDS 0.50 INCH, LOGIC MUST BE CHANGED HERE.
      IF(J-22) 105,368,105
  368 DIR(I,J)=0.
      GO TO 36
  105 CONTINUE
      IF(IWARN-1) 50,51,51
   51 DB=(Y**2-RC**2)**.5
      DA=(Y**2-RD**2)**.5
      THXY=0.
      GO TO 52
   50 DXYS=(X-XCL)**2+Y**2
      DB=(DXYS-RC**2)**.5
      DA=(DXYS-RD**2)**.5
      XMOYM=(XCL-X)/Y
      THXY=ATAN(XMOYM)
   52 CONTINUE
      APB=(A+B)/DA
      THA=ATAN(APB)
      BP=B/DB
      THB=ATAN(BP)
      DOTA=D/(2.*DA)
      COTA=C/(2.*DB)
      THPA=ATAN(DOTA)
      THPB=ATAN(COTA)
      THXAP=THXY+THPA
      THXBP=THXY+THPB
   24 RA=H/SIN(THA)
      RB=H/SIN(THB)
      XAP=RA*COS(THA)/((1.+(TAN(THXAP))**2)**.5)*TAN(THXAP)
      XBP=RB*COS(THB)/((1.+(TAN(THXBP))**2)**.5)*TAN(THXBP)
      YAP=XAP/(TAN(THXAP))
      YBP=XBP/(TAN(THXBP))
      XAL=X-XAP
      XBL=X-XBP
      YAL=Y+YAP
```

```
      YBL=Y+YBP
      IF(IWARN-1) 250,260,260
  250 THXAM=THXY-THPA
      THXBM=THXY-THPB
      XAM=RA*COS(THA)/((1.+(TAN(THXAM))**2)**.5)*TAN(THXAM)
      XBM=RB*COS(THB)/((1.+(TAN(THXBM))**2)**.5)*TAN(THXBM)
      YAM=XAM/(TAN(THXAM))
      YBM=XBM/(TAN(THXBM))
      XAR=X-XAM
      XBR=X-XBM
      YAR=Y+YAM
      YBR=Y+YBM
  260 IF(ICONT-1)25,26,26
   25 CONTINUE
C     CALCULATION OF OBSTRUCTED LAMP COORDINATES
      NP=N/2
      DO 108 ILA=1,NP
      XLA=XI(ILA)
      IF(XLA-XBL)109,109,107
  109 Y1=YBL+(XBL-XLA)/(TAN(THXBP))
      GO TO 13
  107 IF(XLA-XAL)111,111,112
  111 Y1=YAL+(XAL-XLA)*(YBL-YAL)/(XAL-XBL)
      GO TO 13
  112 Y1=Y+(X-XLA)/(TAN(THXAP))
   13 CONTINUE
      IF(Y1-5.)14,14,15
   14 CONTINUE
      IF(IWARN-1) 160,22,22
  160 IF(XLA-XBR) 16,16,17
   16 Y2=YBR+(XBR-XLA)/(TAN(THXBM))
      GO TO 20
   17 IF(XLA-XAR)18,18,19
   18 Y2=YAR+(XAR-XLA)*(YBR-YAR)/(XAR-XBR)
      GO TO 20
   19 Y2=Y+(X-XLA)/(TAN(THXAM))
   20 CONTINUE
      IF(Y2-5.)21,21,22
   22 Y2=5.
   21 CONTINUE
      CALL FAST(X,Y,XLA,Y1,Y2,H,DLP)
      FUN=DLP
      IF(IWARN-1) 161,162,162
  162 DLP=2.*FUN
  161 DIR(I,J)=DIR(I,J)-DLP
   15 CONTINUE
  108 CONTINUE
      ICONT=ICONT+1
      IF(ICONT-1)122,122,23
C     CALCULATION OF OBSTRUCTED REFLECTOR COORDINATES
  122 H=H+R
      GO TO 24
   23 CONTINUE
```

```
 26 DO 28 II=1,46
    CI=II
    XRI=(CI-.5)*.25
    IF(XRI-XBL)30,30,31
 30 YL1=YBL+(XBL-XRI)/(TAN(THXBP))
    GO TO 34
 31 IF(XRI-XAL)32,32,33
 32 YL1=YAL+(XAL-XRI)*(YBL-YAL)/(XAL-XBL)
    GO TO 34
 33 YL1=Y+(X-XRI)/(TAN(THXAP))
 34 CONTINUE
    IF(YL1-5.5)35,35,36
 35 CONTINUE
    IF(IWARN-1) 370,43,43
370 IF(XRI-XBR) 37,37,38
 37 YR2=YBR+(XBR-XRI)/(TAN(THXBM))
    GO TO 41
 38 IF(XRI-XAR)39,39,40
 39 YR2=YAR+(XAR-XRI)*(YBR-YAR)/(XAR-XBR)
    GO TO 41
 40 YR2=Y+(X-XRI)/(TAN(THXAM))
 41 CONTINUE
    IF(YR2-5.5)42,42,43
 43 YR2=5.5
 42 CONTINUE
    DO 29 JJ=1,44
    CJ=JJ
    YRJ=(CJ-.5)*.25-5.5
    IF(YRJ-YL1)45,44,44
 44 IF(YR2-YRJ)45,46,46
 46 H=HIN
    XDS=((X-XRI)/H)**2
    YDS=((Y-YRJ)/H)**2
    PREF=GAD*GAM*RHM*RHO*DX2*DY2/PI
    DEN=(RHM+XDS+YDS)**2
    REFL=PREF*DDIF(II,JJ)/DEN
    IF(IWARN-1) 450,460,460
460 REFL=2.*REFL
450 DIR(I,J)=DIR(I,J)-REFL
 45 CONTINUE
 29 CONTINUE
 36 CONTINUE
 28 CONTINUE
    WRITE(6,610)DIR(I,J)
610 FORMAT(20X,'REDUCED INCIDENT FLUX IS ',E16.8)
104 CONTINUE
103 CONTINUE
    STOP
    END
    SUBROUTINE FICT(X,Y,XL,GA,DI)
    PI=3.1415926
    PSQ=1./(PI**2)
    G=((X-XL)**2+1.)**.5
```

```
      ZEP=GA*(Y+.5)
      ZEM=GA*(Y-.5)
      GS=G**2
      ZPS=ZEP**2
      ZMS=ZEM**2
      PRE=PSQ/(2.*G)
      T1=ZEP/(GS+ZPS)
      T2=-ZEM/(GS+ZMS)
      T3=ATAN(ZEP/G)/G
      T4=-ATAN(ZEM/G)/G
      DI=PRE*(T1+T2+T3+T4)
      RETURN
      END
      SUBROUTINE FAST(X,Y,XLA,Y1,Y2,H,DLP)
      PI=3.1415926
      PSQ=1./(PI**2)
      XSI=(X-XLA)/H
      G=(XSI**2+1.)**.5
      Z1=Y-Y1
      Z2=Y-Y2
      GS=(H*G)**2
      ZS1=Z1**2
      ZS2=Z2**2
      PRE=-PSQ/(2.*G)
      T1=H*Z2/(GS+ZS2)
      T2=-H*Z1/(GS+ZS1)
      ARG3=Z2/(H*G)
      ARG4=Z1/(H*G)
      T3=ATAN(ARG3)/G
      T4=-ATAN(ARG4)/G
      DLP=PRE*(T1+T2+T3+T4)
      RETURN
      END
//GO.SYSIN DD *
   0.375
   0.875
   1.375
   1.875
   2.375
   2.875
   3.375
   4.375
   4.875
   5.375
   5.875
   6.375
   6.875
   7.375
   7.875
   8.375
   8.875
   9.375
   9.875
```

```
10.375
10.875
11.875
12.375
12.875
13.375
13.875
14.375
14.875
15.375
15.875
16.375
16.875
17.375
17.875
18.375
19.375
19.875
20.375
20.875
21.375
21.875
22.375
//
```

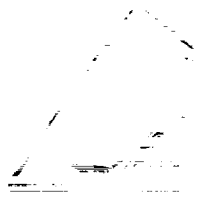

APPENDIX B

DESIGN OF A QUARTZ LAMP THAT PRODUCES UNIFORM DIRECT RADIATION

It would be desirable to develop a lamp geometry that provides a uniform incident flux on the surface beneath it. A system of that type would not be entirely possible if attention is restricted to cylindrical lamps which radiate symmetrically. However, it may be useful to determine the intensity distribution leaving a lamp of finite length, which will provide the most nearly uniform intensity distribution directly beneath it. The intensity distribution leaving the lamp could be controlled by varying the number of turns per centimeter in the tungsten filament. That is, if the tungsten wire is of constant thickness, the intensity leaving the lamp will be direcly proportional to the resistance per centimeter, which is directly proportional to the number of turns per centimeter.

From equation (2), page 4, the intensity distribution directly beneath the lamp is given by

$$\bar{I}(y) = \frac{I_2(o,y)}{\pi I_o} \cdot \frac{H}{D} = r \int_{-\frac{1}{2}}^{\frac{1}{2}} \frac{\bar{I}_1(\bar{\zeta})}{[1 + \gamma^2(\zeta - \bar{\zeta})^2]^2} d\bar{\zeta} \tag{B1}$$

If I_o is selected so that $\bar{I}(y) = r$ is the desired intensity distribution beneath the lamp, the problem would be reduced to finding $\bar{I}_1(\bar{\zeta})$ so that

$$1 = \int_{-\frac{1}{2}}^{\frac{1}{2}} \frac{\bar{I}_1(\bar{\zeta})}{[1 + \gamma^2(\zeta - \bar{\zeta})^2]^2} d\bar{\zeta} \tag{B2}$$

Equations of this type are known as Fredholm integral equations of the first kind (ref. 2). This particular problem could be solved by assuming that $\bar{I}_1(\bar{\zeta})$ takes the form

$$\bar{I}_1(\zeta) = \bar{a}_0 + \bar{a}_1\zeta + \bar{a}_2\zeta^2 + \bar{a}_3\zeta^3 + \ldots \tag{B3}$$

Under this assumption, equation (B1) could be rewritten

$$1 = \sum_{n=0}^{\infty} \bar{a}_n \int_{-\frac{1}{2}}^{\frac{1}{2}} \frac{\bar{\zeta}^n}{[1 + \gamma^2(\zeta - \zeta)^2]^2} d\bar{\zeta} \tag{B4}$$

or

$$1 = \sum_{n=0}^{\infty} \bar{a}_n h_n(\zeta) \tag{B5}$$

where

$$h_n(\zeta) = \int_{-\frac{1}{2}}^{\frac{1}{2}} \frac{\bar{\zeta}^n}{[1 + \zeta^2(\zeta - \bar{\zeta})^2]^2} d\bar{\zeta} \tag{B6}$$

Integrals in the form of equation (B6) could be integrated and yield

$$h_0(\zeta) = \tfrac{1}{2}\left[\frac{(\zeta + \tfrac{1}{2})}{1 + \gamma^2(\zeta + \tfrac{1}{2})^2} - \frac{(\zeta - \tfrac{1}{2})}{1 + \zeta^2(\zeta - \tfrac{1}{2})} + \frac{\tan^{-1}\gamma(\zeta + \tfrac{1}{2})}{\gamma} - \frac{\tan^{-1}\gamma(\zeta - \tfrac{1}{2})}{\gamma}\right] \tag{B7}$$

$$h_1(\zeta) = \frac{1}{2\gamma^2}\left\{\frac{1 + \gamma^2\zeta(\zeta + \tfrac{1}{2})}{1 + \gamma^2(\zeta + \tfrac{1}{2})^2} - \frac{1 + \gamma^2(\zeta - \tfrac{1}{2})\zeta}{1 + \gamma^2(\zeta - \tfrac{1}{2})^2} + \gamma\zeta\left[\tan^{-1}\gamma(\zeta + \tfrac{1}{2}) - \tan^{-1}\gamma(\zeta - \tfrac{1}{2})\right]\right\} \tag{B8}$$

$$h_2(\zeta) = \frac{1}{2\gamma^2}\left\{\frac{\gamma^2\zeta^2(\zeta + \tfrac{1}{2}) + (\zeta - \tfrac{1}{2})}{1 + \gamma^2(\zeta + \tfrac{1}{2})^2} - \frac{\gamma^2\zeta^2(\zeta - \tfrac{1}{2}) + (\zeta + \tfrac{1}{2})}{1 + \gamma^2(\zeta - \tfrac{1}{2})^2} + \frac{1 + \gamma^2\zeta^2}{\gamma}\left[\tan^{-1}\gamma(\zeta + \tfrac{1}{2}) - \tan^{-1}\gamma(\zeta - \tfrac{1}{2})\right]\right\} \tag{B9}$$

and so on.

The obvious problem which remains to be solved is the calculation of coefficients $\bar{a}_n$ in equation (B4). Morse and Feshback (ref. 3) have shown that the series in equation (B3) is not a useful form because of the difficulty in evaluating the $\bar{a}_n$. Rather, the series should have been written in the form of

$$\bar{I}_1(\zeta) = a_0 + a_1(\zeta + \alpha_{10}) + a_2(\zeta^2 + \alpha_{21}\zeta + \alpha_{20}) + a_3(\zeta^3 + \alpha_{32}\zeta^2 + \alpha_{31}\zeta + \alpha_{30}) + \ldots \tag{B10}$$

Under these conditions, equation (B6) takes the form

$$1 = a_0 h_0(\zeta) + a_1\left[h_1(\zeta) + \alpha_{10}h_0(\zeta)\right] + a_2\left[h_2(\zeta) + \alpha_{21}h_1(\zeta) + \alpha_{20}h_0(\zeta)\right] + \ldots \tag{B11}$$

The basis for this polynomial expansion is that the Gram-Schmidt orthogonalization procedure could be used to construct orthogonal functions $\psi_n(\zeta)$ from the $h_n(\zeta)$ by

$$\psi_0(\zeta) = h_0(\zeta)$$

$$\psi_1(\zeta) = h_1(\zeta) + \alpha_{10}h_0(\zeta)$$

$$\psi_2(\zeta) = h_2(\zeta) + \alpha_{21}h_1(\zeta) + \alpha_{20}h_0(\zeta)$$

.

.

$$\psi_n(\zeta) = h_n(\zeta) + \sum_{i=0}^{n-1} \alpha_{ni} h_i(\zeta) \tag{B12}$$

If the inner product is defined by

$$(f,g) = \int_{-\frac{1}{2}}^{\frac{1}{2}} f(\bar{\zeta}) g(\bar{\zeta}) d\bar{\zeta}, \tag{B13}$$

$\psi_0(\zeta)$ and $\psi_1(\zeta)$ are orthogonal if

$$\int_{-\frac{1}{2}}^{\frac{1}{2}} \psi_0(\bar{\zeta}) \psi_1(\bar{\zeta}) d\bar{\zeta} = 0 = (h_1, \psi_0) + \alpha_{10} \|\psi_0\|^2 \tag{B14}$$

where

$$\|\psi_0\|^2 = \int_{-\frac{1}{2}}^{\frac{1}{2}} \psi_0^2(\bar{\zeta}) d\bar{\zeta} \tag{B15}$$

Obviously, equation (B14) would be satisfied if α_{10} were given by

$$\alpha_{10} = \frac{-(h_1, \psi_0)}{\|\psi_0\|^2} \tag{B16}$$

Similarly, α_{21} and α_{20} are given by

$$\alpha_{21} = \frac{-(h_2, \psi_1)}{\|\psi_1\|^2}$$

and

$$\alpha_{20} = \frac{-(h_2, \psi_0)}{\|\psi_0\|^2} \tag{B17}$$

These quantities were evaluated by numerically integrating the appropriate inner products.

The magnitudes of α_{10} and α_{21} are negligibly small when compared with the numerical integration accuracy. The value of α_{20} is a function of γ and is tabulated below:

OPTIMIZATION COEFFICIENTS FOR UNIFORM DIRECT RADIATION

γ	α_{20}	a_0	a_2	$\bar{a}_0$	β
2	-.070586	1.769	18.100	0.491	36.864
4	-.067466	2.947	11.704	2.157	5.426
6	-.068425	4.186	10.257	3.484	2.944
8	-.069984	5.433	9.702	4.764	2.037
10	-.071436	6.706	9.434	6.032	1.564
20	-.075908	13.054	9.092	12.364	0.7354
40	-.079131	25.777	9.058	25.060	0.3615
60	-.080364	38.507	9.086	37.777	0.2405
80	-.080994	51.239	9.148	50.498	0.1812
100	-.081360	63.975	9.290	63.219	0.1469

If the uniform intensity distribution is to be approximated by

$$\bar{I}_1(\zeta) \simeq \bar{a}_0 + \bar{a}_1\zeta + \bar{a}_2\zeta^2 \tag{B18}$$

it is necessary to regroup the first three terms in equation (B10). That is, if $\bar{I}_1(\zeta)$ is approximated by

$$\bar{I}_1(\zeta) \simeq a_0 + a_1\zeta + a_2(\alpha_{20} + \zeta^2) \tag{B19}$$

where a_0, a_1, and a_2 are given by

$$a_0 = \frac{(\psi_0,1)}{\|\psi_0\|^2}, \quad a_1 = \frac{(\psi_1,1)}{\|\psi_1\|^2}, \quad \text{and} \quad a_2 = \frac{(\psi_2,1)}{\|\psi_2\|^2} \tag{B20}$$

an approximate set of values for $\bar{a}_0$, $\bar{a}_1$, and $\bar{a}_2$ could be developed. Numerical integration of the expressions in equation (B20) shows that a_1 is negligibly small and that a_0 and a_2 vary with γ. These quantities along with $\bar{a}_0$ are also tabulated above. (Note that $\bar{a}_2 = a_2$.)

If $\bar{I}_1(\zeta)$ is written

$$I_1(\zeta) = \bar{a}_0(1 + \beta\zeta^2) \tag{B21}$$

the relative importance of the quadratic term is indicated by β and is shown in the table above. It can be seen that for large values of γ (long lamps close to the surface), the nonuniform term becomes small; whereas for small values of γ (short lamps away from the surface), the uniform contribution is small and the lamps should essentially be unheated at their centers.

REFERENCES

1. LaToison, M.: Infrared and Its Thermal Applications. Gordon and Breach, Science Publications, 1964, pp. 66-68.

2. Morse, P. M.; and Feshback, H.: Methods of Theoretical Physics, McGraw-Hill Book Company, Inc., 1953, pp. 896-997.

3. *Ibid.*, pp. 925-931.

REPORT DOCUMENTATION PAGE

Form Approved
OMB No. 0704-0188

1. AGENCY USE ONLY (*Leave blank*)	2. REPORT DATE	3. REPORT TYPE AND DATES COVERED
	June 1972	Contractor Report

4. TITLE AND SUBTITLE
An Analysis of the Radiation Field Beneath a Bank of Tubular Quartz Lamps

5. FUNDING NUMBERS
C NAS1-9434, Task 34
WU 505-63-50-10

6. AUTHOR(S)
Robert L. Ash

7. PERFORMING ORGANIZATION NAME(S) AND ADDRESS(ES)
Old Dominion University
Norfolk, VA 23529

8. PERFORMING ORGANIZATION REPORT NUMBER
TR 72-T3

9. SPONSORING / MONITORING AGENCY NAME(S) AND ADDRESS(ES)
National Aeronautics and Space Administration
Washington, DC 20546-0001

10. SPONSORING / MONITORING AGENCY REPORT NUMBER
NASA CR-191551

11. SUPPLEMENTARY NOTES

12a. DISTRIBUTION / AVAILABILITY STATEMENT
Unclassified - Unlimited

Subject Category: 34

12b. DISTRIBUTION CODE

13. ABSTRACT (*Maximum 200 words*)

Equations governing the incident heat flux distribution beneath a lamp-reflector system have been developed. Analysis of a particular radiant heating facility showed good agreement between theory and experiment when a lamp power loss correction was used. In addition, the theory was employed to estimate thermal disruption in the radiation field caused by a protruding probe.

14. SUBJECT TERMS
Quart Heaters; Infrared Heaters; Thermal Radiation; Heat flux; Reflectors; Radiant intensity

15. NUMBER OF PAGES
34

16. PRICE CODE
A03

17. SECURITY CLASSIFICATION OF REPORT	18. SECURITY CLASSIFICATION OF THIS PAGE	19. SECURITY CLASSIFICATION OF ABSTRACT	20. LIMITATION OF ABSTRACT
Unclassified	Unclassified		